Supporting Information

20.46% Efficient Organic Solar Cells with Concurrent Voltage Enhancement and Thermal Stability Enabled by Crystallization-Kinetics-Controlled Morphology

Anhai Liang[†],[1] Chunliang Li[†],[2] Bosen Zou,[2] Sein Chung,[3] Byeongjin Kim,[3] Yongjoon Cho,[4] Jiancheng Zhong,[1] Jingjing Zhao,[1] Lixing Tan,[1] Guangquan Zhang,[1] Xin Li,[1] Wuning Wei,[1] Kilwon Cho,[3] He Yan,[2*] Zhipeng Kan[1*]*

[1] Center on Nanoenergy Research, Institute of Science and Technology for Carbon Peak & Neutrality, School of Physical Science & Technology, Guangxi University, Nanning 530004, China.

[2] Department of Chemistry and Hong Kong Branch of Chinese National Engineering Research Center for Tissue Restoration and Reconstruction, The Hong Kong University of Science and Technology, Hong Kong 999077, China.

[3] Department of Chemical Engineering, Pohang University of Science and Technology, Pohang 37673, Republic of Korea.

[4]Department of Physics and Chemistry, Daegu Gyeongbuk Institute of Science and Technology (DGIST), Daegu 42988 Republic of Korea

Email: bzouaa@connect.ust.hk; hyan@ust.hk

Email: kanzhipeng@gxu.edu.cn

[†] These authors contributed equally to this work. Supporting information for this article is given via a link at the end of the document.

General Information.

^{1}H and ^{13}C NMR spectra were recorded on a Bruker AV-400 MHz NMR spectrometer. Chemical shifts were reported in parts per million (ppm, δ). Mass spectra were collected on a MALDI Micro MX mass spectrometer, or an API QSTAR XL System.

Experimental Materials.

All chemicals, unless otherwise specified, were purchased from Energy or other commercial resources and used as received. The starting materials (BTP-BO-CHO, IC-F) are commercially available. PM6 and PDIN were purchased from Organtec Ltd. L8-BO was purchased from Hyper PV Technology Co., Ltd. PEDOT:PSS (CLEVIOSTM P VP AI 4083, Heraeus, Germany) was purchased from Xi'an Yuri Solar Co., Ltd. All materials were used as received without further purification. The synthesis steps of the end groups (IC-ClO) are similar to our previous report.[1]

Solar cell fabrication

Binary and ternary OSCs were prepared by ITO/PEDOT: PSS/ active layer /PDIN/Ag. The glass substrate was coated with indium tin oxide (ITO, device area: 0.04 cm^2). Ultrasonic cleaning of the substrate was performed in the order of dishwashing liquid, deionized water, acetone, deionized water and isopropyl alcohol for 15 minutes each. The ITO glass was then treated in an ultraviolet-ozone cleaner for 30 minutes. A layer of PEDOT: PSS (~30 nm) (CLEVIOSTM P VP AI 4083, Heraeus, Germany) was applied to the UV-treated ITO base by a static spin coating method, and the base is then transferred to the glove box for active layer deposition. All solutions were prepared with polymer donors (PM6) and acceptors (L8-BO and BTP-FClO) in a nitrogen-filled glove box. The D:A (donor:acceptor) ratio was maintained at 1:1.2 with a total concentration of 18 mg/mL, were dissolved in chloroform (CF), heated and stirred on a magnetic stirrer for 2 hours, and the active layer solution was spin coated at 3000 rpm. Then PDIN solution (2.0 mg/mL in methanol with 0.3 vol% acetic acid) was spin-coated on the top of the active layer as the electron transport layer. The device is then placed in a high vacuum environment of 7×10^{-7} Torr, where Ag (100 nm) is thermally evaporated onto the active layer.

UV-Vis Absorption.

UV-Vis absorption spectra of different blend films were recorded on a PerkinElmer LAMBDA 365 UV-Vis spectrophotometer.

Photoluminescence characterizations

The photoluminescence of the films was measured by a FLS1000 equipped with an integrating hemisphere at an excitation wavelength of 500 nm and 630 nm from Edinburgh Instruments Co., Ltd.

Contact angle measurements

The contact angles of the neat film and the blended film were performed on the L2004A1 (Ossila England) contact Angle instrument.Then the surface free energy was calculated by Owens-Wendt method:

$$\varepsilon_L \times (1 + \cos\theta) = 2 \times (\varepsilon_L^d \cdot \varepsilon_{SV}^d)^{1/2} + 2 \times (\varepsilon_L^p \cdot \varepsilon_{SV}^p)^{1/2}$$

Where ε_L and ε_{SV} are the surface free energies of the sample film in different liquids (deionized water and formamide), θ is the contact Angle of the sample, the average contact Angle and surface energy parameters obtained through video dynamic analysis are shown in Table S1 and Table S2. Then the Flory Huggins interaction parameter $\chi_{donor\text{-}acceptor}$ of the blend is calculated to show the compatibility of the blend films, which can be obtained from the following formula:

$$\chi_{donor-acceptor} = K(\gamma_{donor}^{1/2} - \gamma_{acceptor}^{1/2})^2$$

where *γ* is the surface energy of the material, K is the proportionality constant.

Photocurrent measurements.

The *J-V* measurement was performed via a XES-50S1 (SAN-EI Electric Co., Ltd.) solar simulator (AAA grade) whose intensity was calibrated by a certified standard silicon solar cell (SRC-2020, Enlitech) under illumination of AM 1.5G 100 mW cm^{-2}. The AM 1.5G light source with a spectral mismatch factor of 1.01 was calibrated by the National Institute of Metrology. The intensity of the AM 1.5G

spectra was calibrated by a certified standard silicon solar cell (SRC-2020, Enlitech) calibrated by the National Institute of Metrology. The *J-V* curves of small-area devices were measured in forwarding scan mode (from -0.2 V to 1.2 V) with a scan step length of 0.02 V.

External quantum efficiency (EQE) measurements.

The external quantum efficiency (EQE) was measured by a certified incident photon to electron conversion (IPCE) equipment (QE-R) from Enli Technology Co., Lt. The light intensity at each wavelength was calibrated using a standard monocrystalline Si photovoltaic cell.

SCLC Measurements

The carrier mobility (hole and electron mobility) of the photoactive layer was measured by fitting the dark current of the hole/electron diode with the space charge limited current (SCLC) model. The scan started from -5 V to 5 V. The measurements of pure electronic devices and pure hole devices are prepared. Electronic device structure of ITO/ZnO/BHJ/PDIN/Ag and only hole of ITO/PEDOT: PSS/BHJ/MoO3/Ag. The single-carrier device was connected to a Source Measure Unit (Keithley, Model 236 SMU) which provides DC9 voltage to the electron-only devices. The *J–V* values of different DC voltages can bedetected and recorded through SMU. The J-V characteristics were further analyzed by the space-charge-limited-current (SCLC) method to extract zero-field carrier mobilities, where SCLC is described by:

$$J = \frac{9\varepsilon_0\varepsilon_\gamma\mu_0 V^2}{8L^3} exp(0.89\beta\sqrt{\frac{V}{L}})$$

where J is the current density, L is the film thickness of the active layer, μ_0 is the hole or electron mobility, ε_r is the relative dielectric constant of the transport medium, ε_0 is the permittivity of free space (8.85×10^{-12} F m^{-1}), V (= V_{appl} - V_{bi}) is the internal voltage in the device, where V_{appl} is the applied voltage to the device and V_{bi} is the built-in voltage due to the relative work function difference of the two electrodes.

Carrier extraction by linearly increasing voltage (CELIV)

According to the composite model of Mozer et al., the change of carrier density n(t) with time can be expressed as:

$$n(t) = \frac{n_0}{1 + (\frac{t}{\tau_b})^{\gamma}}$$

Where n(t) is the charge density at time t, n_0 is the initial charge density, τ_b is the recombination lifetime, and γ is the dispersion parameter. γ closes to 1, indicating a nondispersive bimolecular recombination at room temperature. The closer γ is to 1, the fewer traps there are in the system, and the slower the rate of bimolecular recombination. In the dispersive bimolecular recombination, the decay of carrier density is given by:

$$\beta(t) = -\frac{dn(t)/d(t)}{n^2(t)}$$

where n(t) is the carrier density and β(t) is dispersive bimolecular recombination rate at a delay time t. Substituting the first equation, the bimolecular recombination rate β(t) can also be expressed as:

$$\beta(t) = \left(\frac{1}{\tau_b}\right)\gamma {n_0}^{-1}(t/\tau_b)^{\gamma-1}$$

The resulting β(t) can be calculated from the fitting parameters n_0, τ_b and γ using equation above.

Empirical relationship between the V_{oc} and FF

The correlation between the V_{oc} and the maximum fill factor (FF_{max}) in a specific device can be characterized as follows:[35-37]

$$FF_{max} = \frac{\gamma_{oc} - \ln(\gamma_{oc} + 0.72)}{\gamma_{oc} + 1}$$

$$\gamma_{oc} = \frac{qV_{OC}}{nkT}$$

Where q is the elementary charge, n is the diode ideality factor, k is the Boltzmann constant, and T is the temperature. It has been observed that the FF achieved in high performance organic solar cells (OSCs) typically falls within the range of FF_{max} - (0.10 ± 0.04), as documented in prior studies.

Atomic Force Microscopy (AFM)

A Dimension Icon atomic force microscope (AFM) from Bruker was used to image the active layers in tapping mode. The glass substrate is exposed to ultraviolet ozone plasma for 15 minutes

and spin coated directly in a nitrogen environment. The atomic force microscope is used for non-contact scanning, and the cantilever oscillates at a distance of 5 ~ 10 nm above the sample surface when detecting the sample surface. By continuously changing the scale from 500 μm to 5 nm, the surface morphology of the film was observed, and finally the AFM image with the size of 2 x 2 μm was captured.

Transmission Electron Microscopy (TEM)

A layer of PEDOT: PSS is applied to the base, and then spin the film. The glass substrate was placed on the surface of deionized water, dissolved in water using the hydrophilicity of the PEDOT: PSS layer, then transferred to a 50-mesh copper grid on the substrate (China Electron Microscope), and corrected electron microscope (Titan ETEM G2 E-Twin) by spherical aberration observation at an accelerated operating voltage of 300kev.

Grazing Incidence Wide-angle X-ray Scattering

Swept wide-angle X-ray scattering (GIWAXS), beamlines 3C SAXS-I and 9A U-SAXS were measured at the Pohang Light Source in South Korea. After careful selection, the incidence Angle is 0.12° to ensure that the X-ray completely penetrates the film. The e film is prepared according to the method described in the section on Device Fabrication. Using Scherrer equation to calculate coherence length (CCL) Peak CCL = $2\pi k/\Delta q$, where k is a dimensionless shape factor (where k = 0.9) and Δq is the full half-peak width (FWHM) of a given peak.

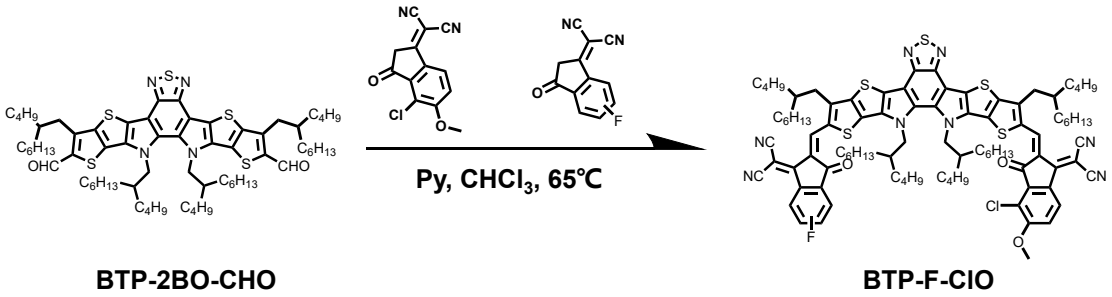

BTP-2BO-CHO **BTP-F-ClO**

Fig. S1 Synthesis routes of **BTP-F-ClO**.

Synthesis of **BTP-F-ClO**

BTP-2BO-CHO (200 mg, 0.172 mmol), **IC-ClOMe** (44.5 mg, 0.172 mmol), **IC-F** (36.5 mg, 0.172 mmol) were dissolved in absolute chloroform (10 mL), and pyridine (1.5 mL) were added. The mixture was deoxygenated with nitrogen for 30 min and then refluxed for 4 h. After cooling to room temperature, the mixture was poured into methanol (100 mL) and filtered. The residue was purified by column chromatography on silica gel using petroleum ether/dichloromethane (1:1.5) as eluent, yielding a dark blue solid and recrystallization through MeOH/DCM for two times to obtain **BTP-F-ClO** (158 mg, 57%). **^{1}H NMR** (400 MHz, $CDCl_3$) δ 9.15 (d, *J* = 6.3 Hz, 2H), 8.69 (d, *J* = 8.7 Hz, 1H), 8.41 (dd, *J* = 9.0, 2.0 Hz, 1H), 7.94 (dd, *J* = 8.3, 5.2 Hz, 1H), 7.24 (d, *J* = 8.9 Hz, 1H), 4.85 – 4.65 (m, 4H), 4.09 (s, 3H), 3.19 (d, *J* = 7.5 Hz, 4H), 2.24 – 1.94 (m, 4H), 1.48 – 0.57 (m, 88H). ^{13}C NMR (101 MHz, $CDCl_3$) δ 186.30, 185.42, 164.77, 159.42, 159.24, 158.67, 152.46, 152.17, 146.92, 144.56, 144.52, 141.77, 141.67, 137.13, 136.83, 135.01, 134.89, 134.75, 133.56, 133.44, 133.30, 133.02, 132.52, 130.05, 125.04, 124.48, 120.99, 120.78, 120.24, 120.10, 115.48, 115.17, 114.87, 114.66, 113.96, 112.87, 112.61, 112.23, 111.97, 68.22, 65.51, 56.55, 55.16, 54.96, 39.40, 38.53, 34.09, 34.01, 32.92, 32.67, 31.24, 30.89, 30.85, 29.80, 29.04, 28.77, 28.72, 28.70, 28.22, 27.21, 25.95, 24.80, 24.69, 22.40, 22.39, 22.21, 22.17, 22.14, 22.03, 21.82, 21.80, 13.47, 13.38, 13.33, 13.12, 13.09.MS (CI) [M] calcd. for ($C_{93}H_{110}FClN_8O_3S_5$): 1602.7. Found:1601.7.

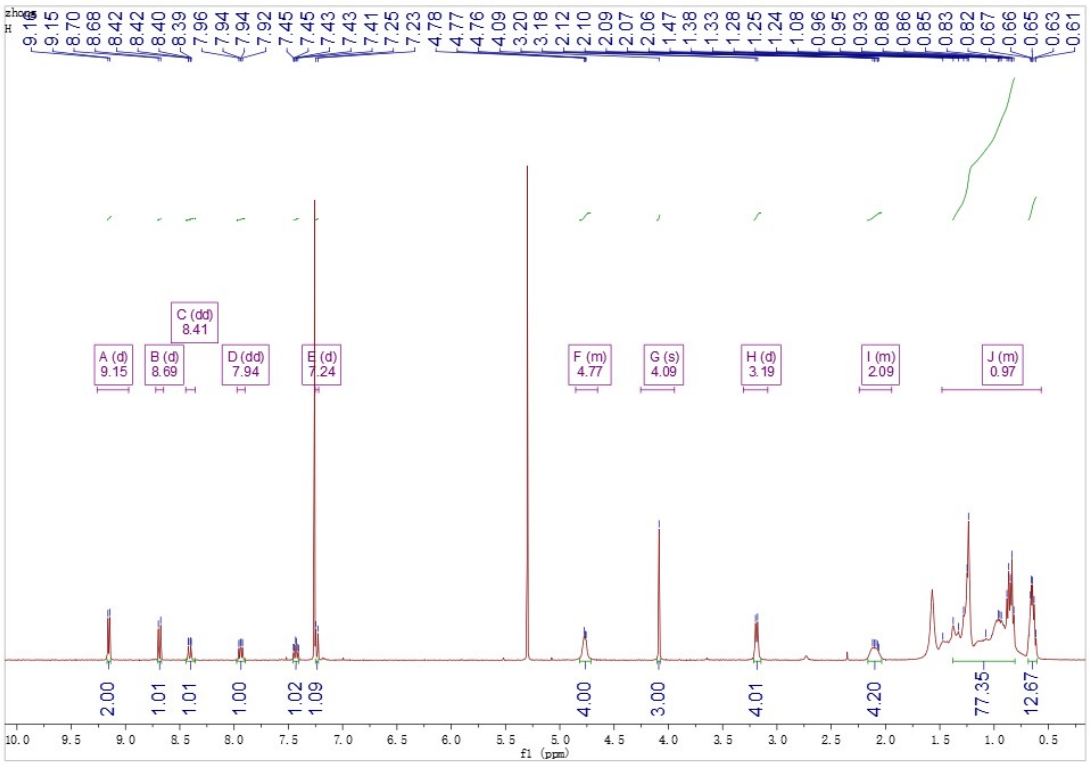

Fig. S2. ^{1}H NMR spectrum of **BTP-F-ClO** (400 MHz, $CDCl_3$).

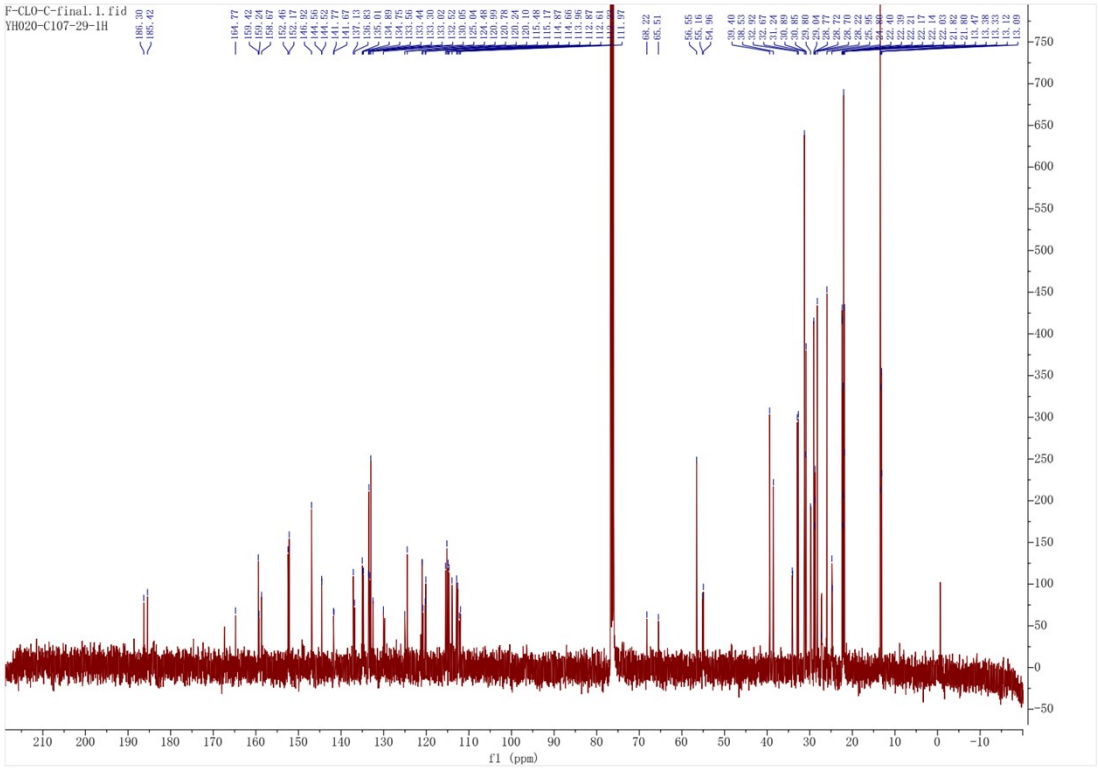

Fig. S3. ^{13}C NMR spectrum of **BTP-F-ClO** (400 MHz, $CDCl_3$).

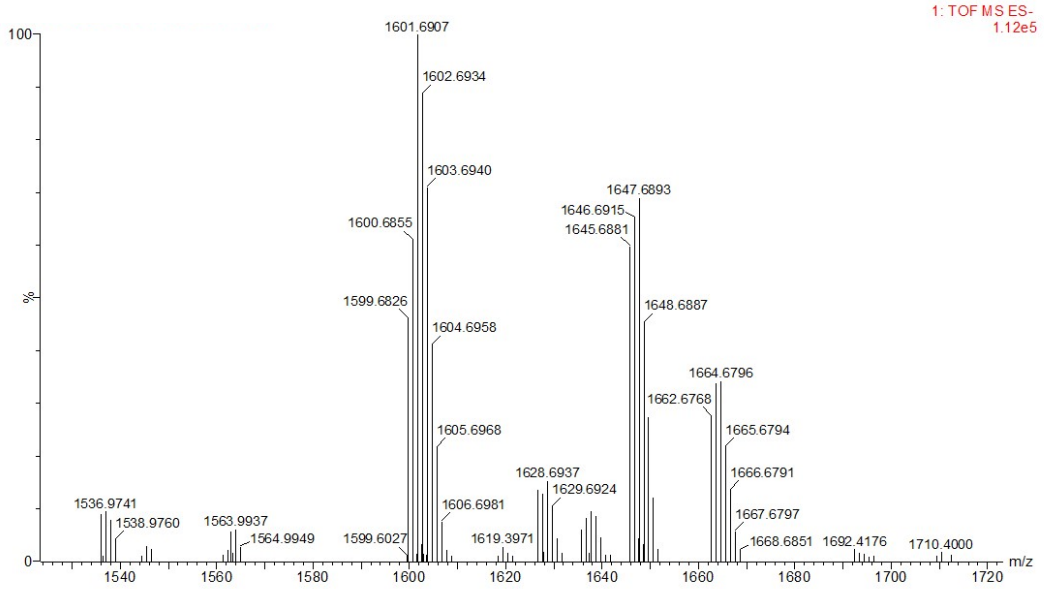

Fig. S4. MS spectrum of **BTP-F-ClO**.

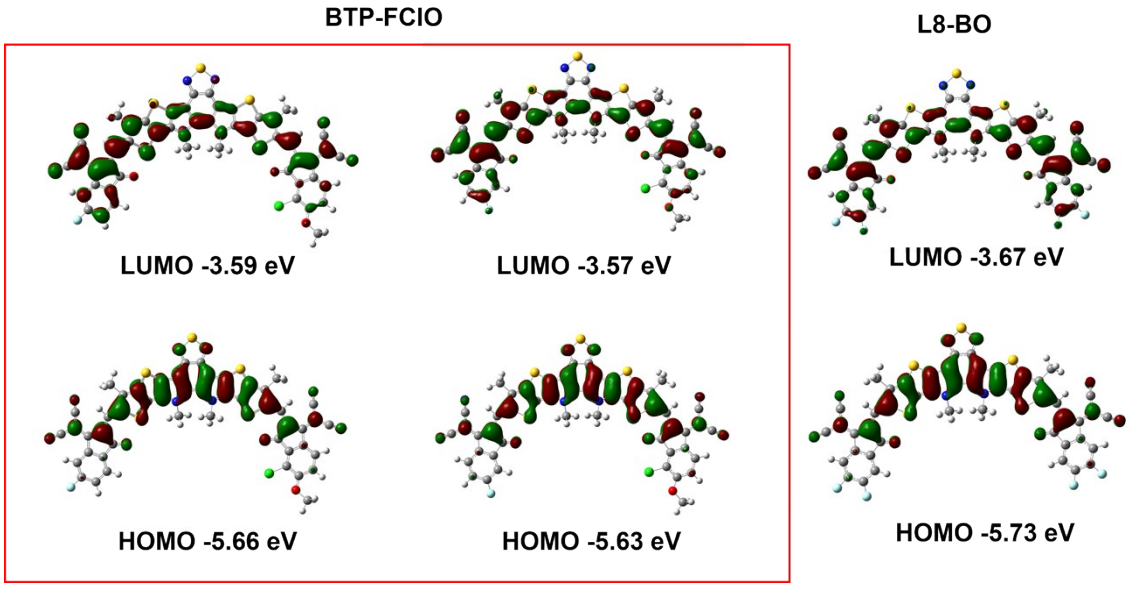

Fig. S5. Theory calculation results of possible sub-units of BTP-FClO and L8-BO

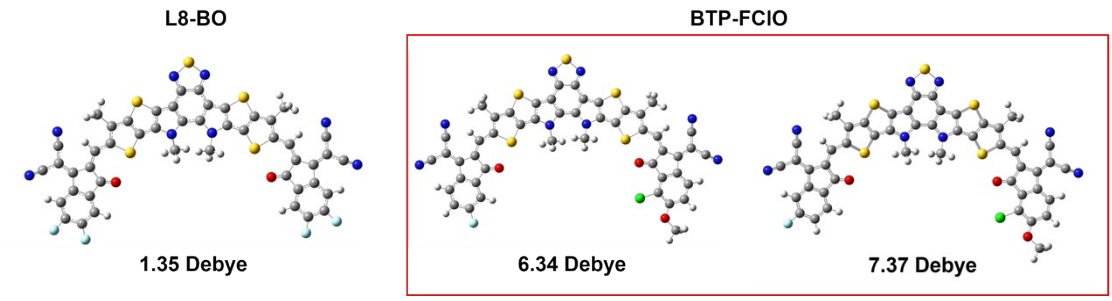

Fig. S6. Molecular structures and corresponding dipole moment values for L8-BO and BTP-FCIO.

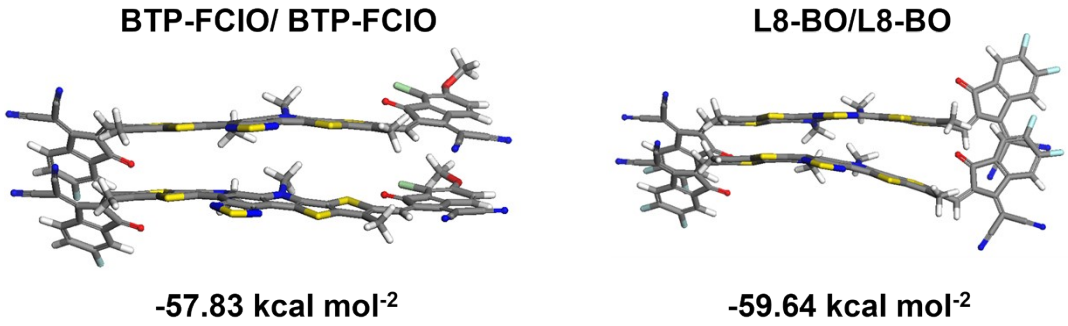

Fig. S7. Molecular structures and binding energies of homodimers.

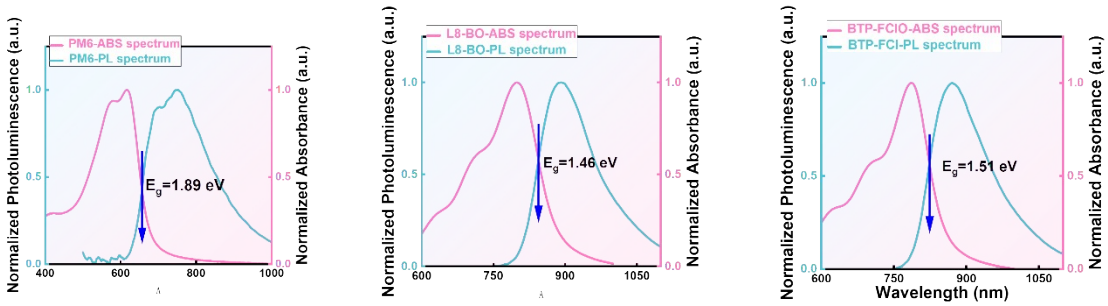

Fig. S8. Normalized absorbance and photoluminescence spectra of the PM6, L8-BO and BTP-FClO.

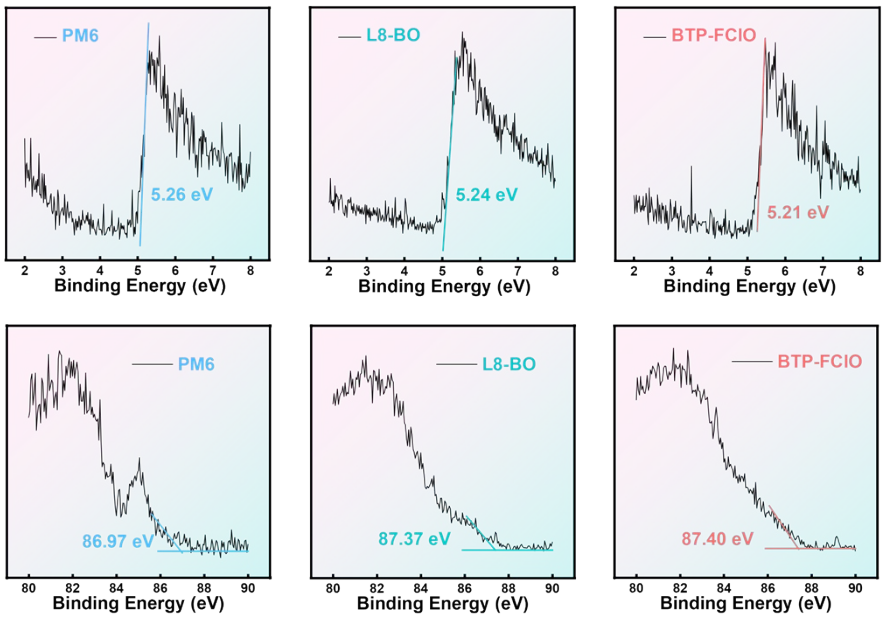

Fig. S9. Ultraviolet photoelectron spectroscopy (UPS) of three neat films.

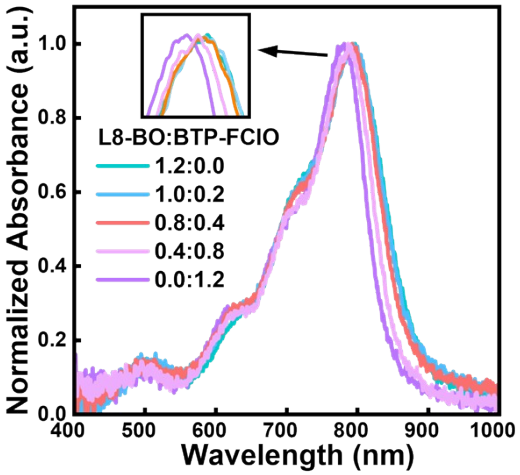

Fig. S10. The absorbance spectra of L8-BO:BTP-FClO binary blends at varying weight ratios.

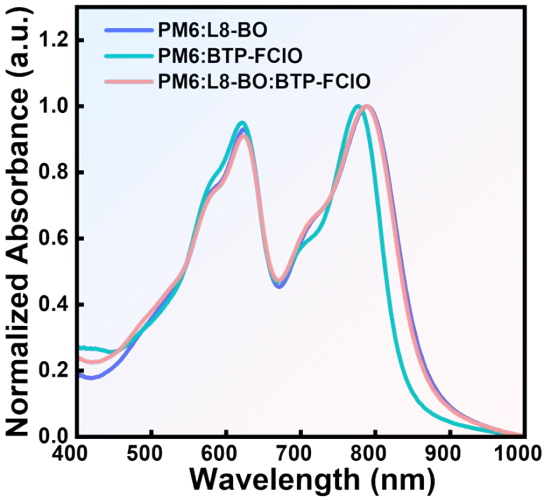

Fig. S11. Normalized absorbance spectra of blend films.

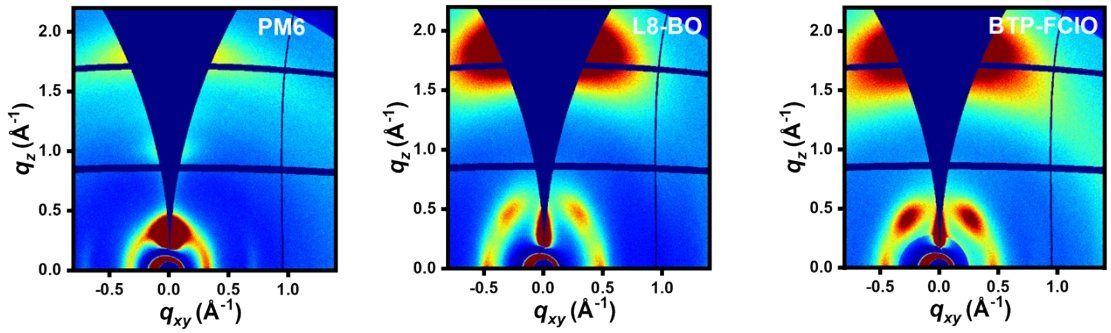

Fig. S12. Grazing-Incidence Wide-Angle X-ray Scattering of three neat films.

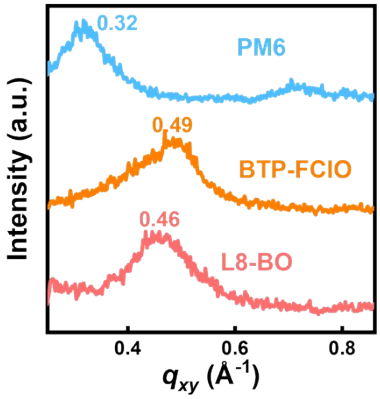

Fig. S13. The in-plane (IP) of three neat films.

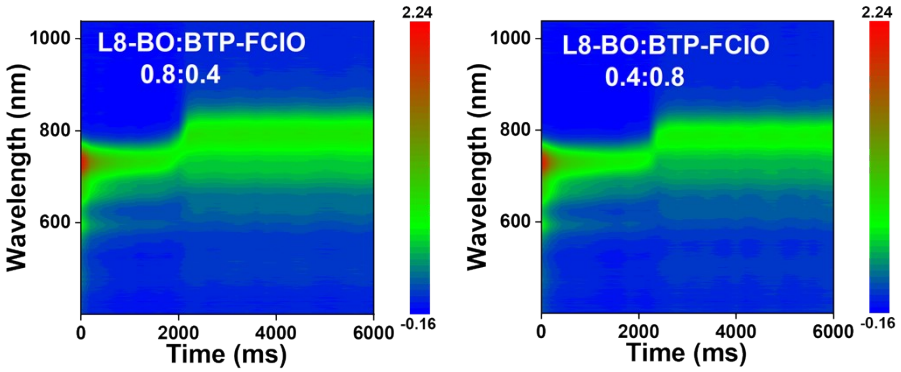

Fig. S14. In situ 2D UV/Vis absorption for different acceptor ratios.

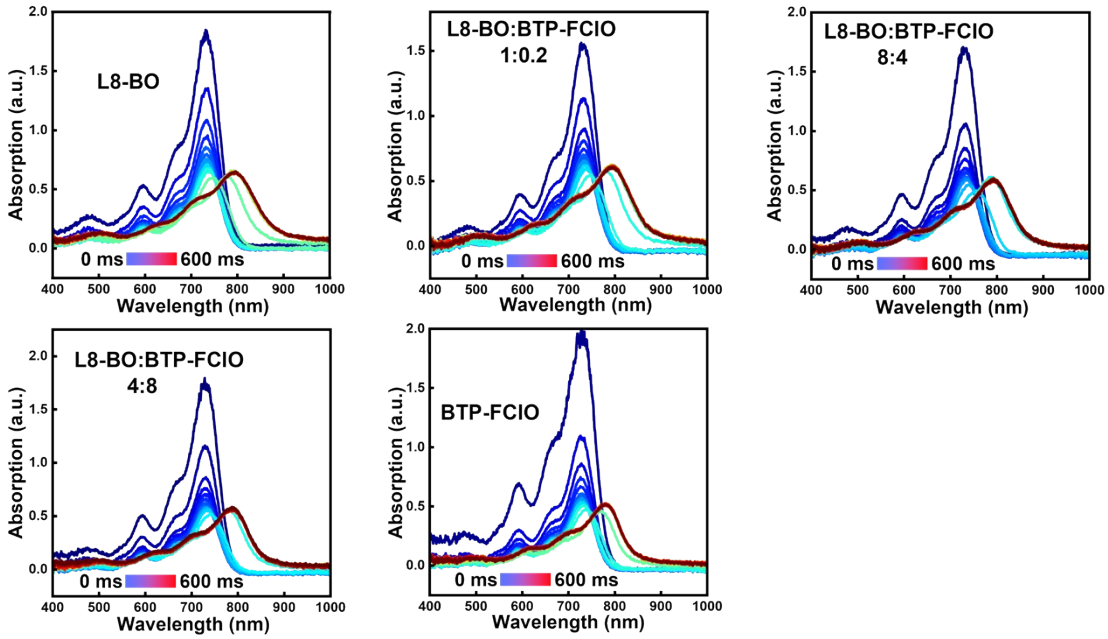

Fig. S15. Transient absorption spectra of acceptors with different ratios

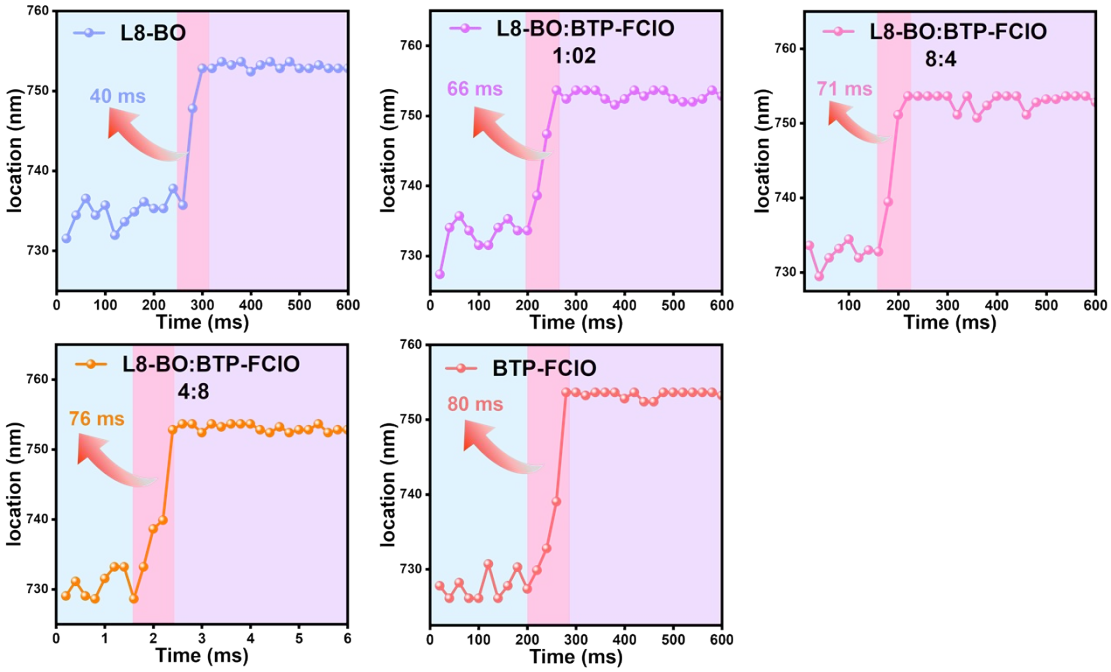

Fig. S16. Temporal evolution of peak positions for different acceptors during the spin-coating process.

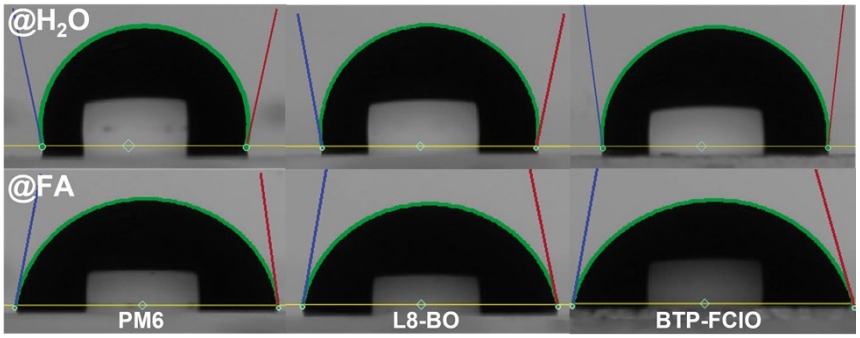

Fig. S17. Contact angle measurements of the neat films.

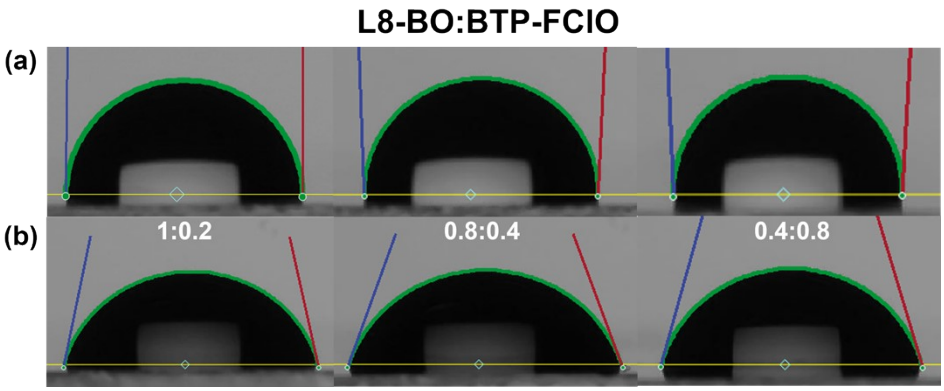

Fig. S18. Contact angle measurements for different acceptor ratios: (a) Water, (b) FA.

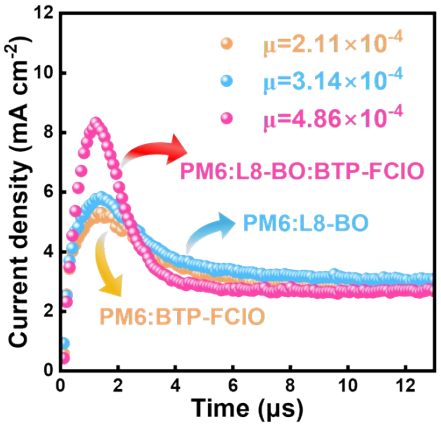

Fig. S19. The photon-induced charge-carrier extraction in linearly increasing voltage (photo-CELIV) measurement.

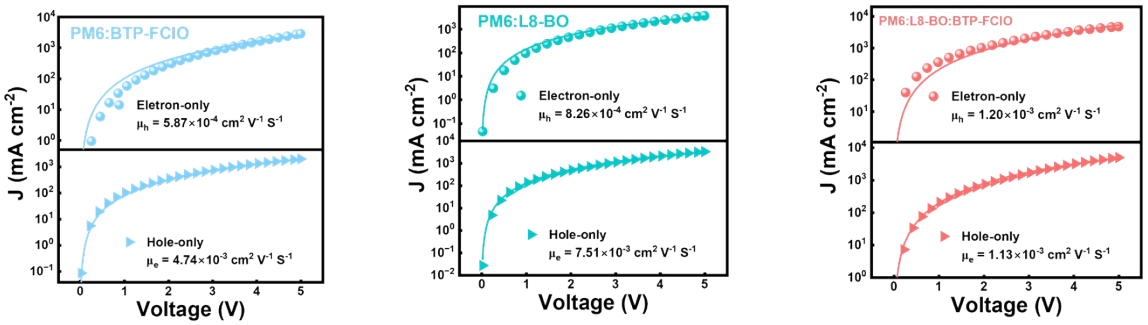

Fig. S20. The hole and electron mobility of binary and ternary devices.

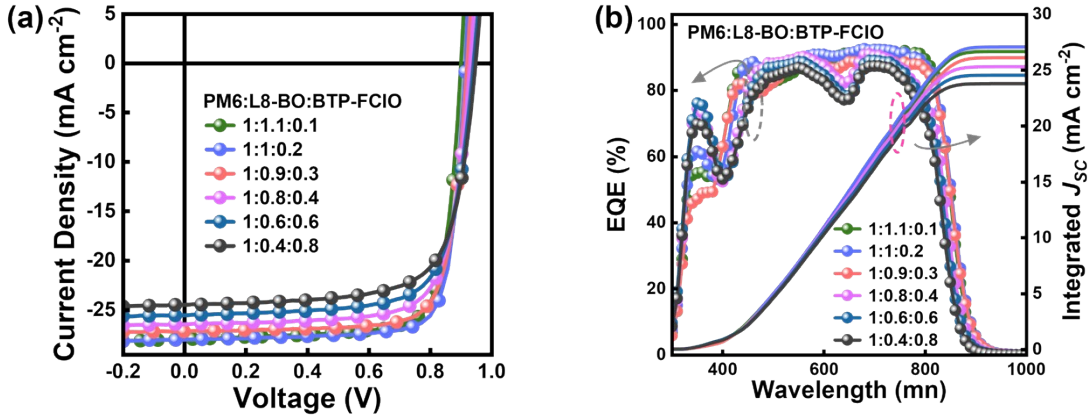

Fig. S21. (a) J-V curves of the binary and ternary OSCs. (b) External quantum efficiency spectra.

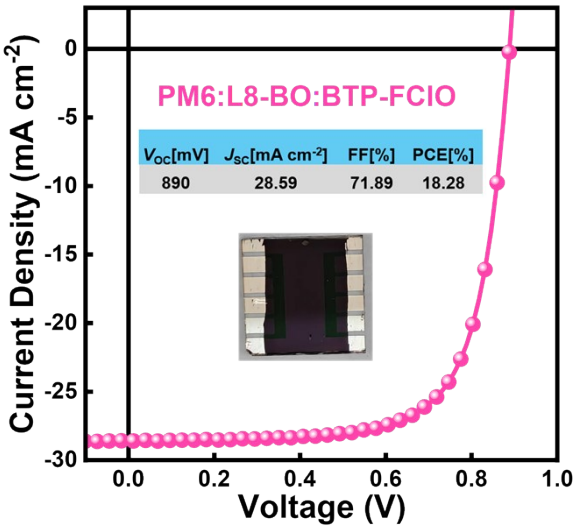

Fig. S22. Current density-voltage (J-V) characteristics of PM6:L8-BO:BTP-FClO.

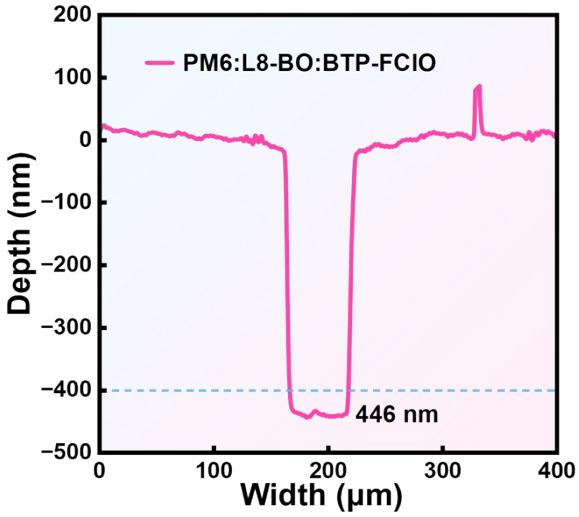

Fig. S23. Surface depth profile curve of PM6:L8-BO:BTP-FClO by stylus profilometry.

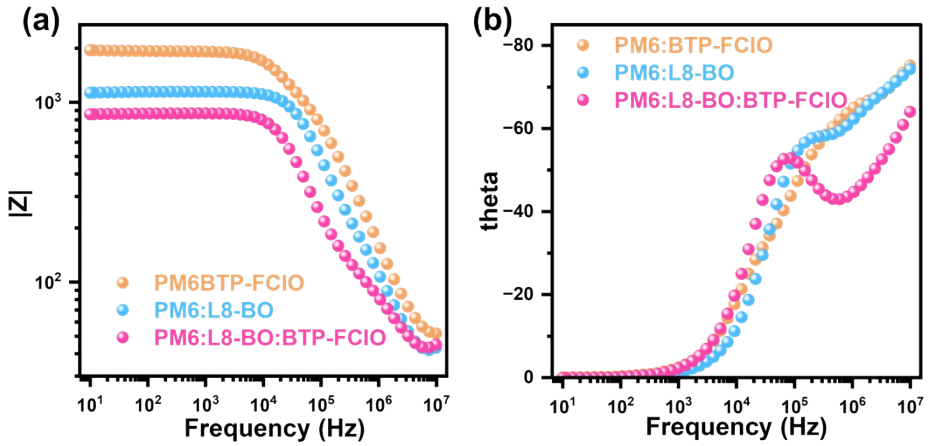

Fig. S24. Bode plots for the different active layer systems: (a) phase angle and frequency. (b) impedance modulus |Z| and frequency.

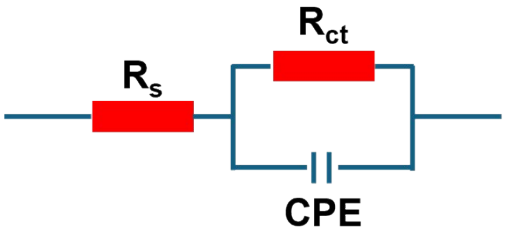

Fig. S25. Equivalent circuit model used for fitting the electrochemical impedance spectroscopy (EIS) data.

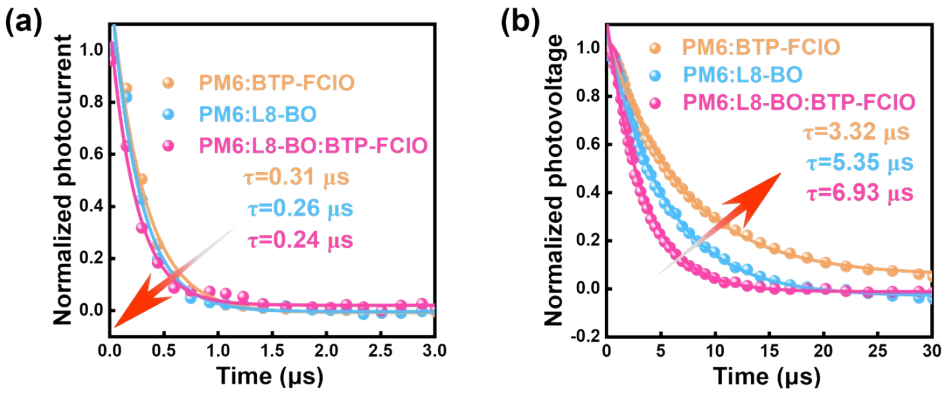

Fig. S26. (a) Transient photocurrent. (b)Transient photovoltage.

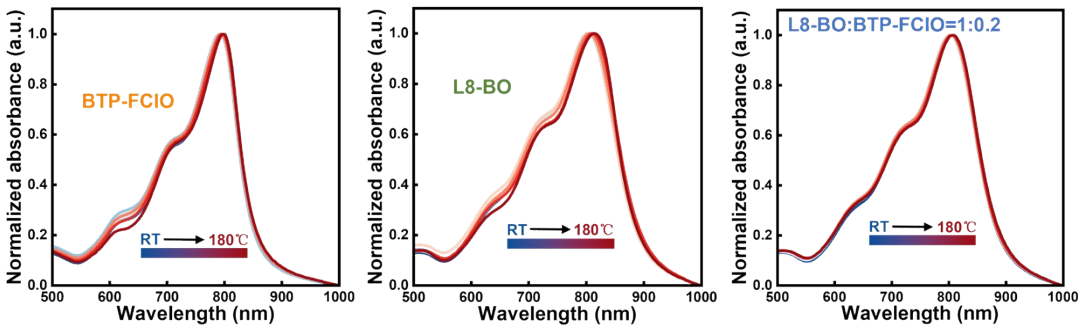

Fig. S27. Temperature varied thermally annealed film's absorption spectra of L8-BO, BTP-FClO and L8-BO:BTP-FClO.

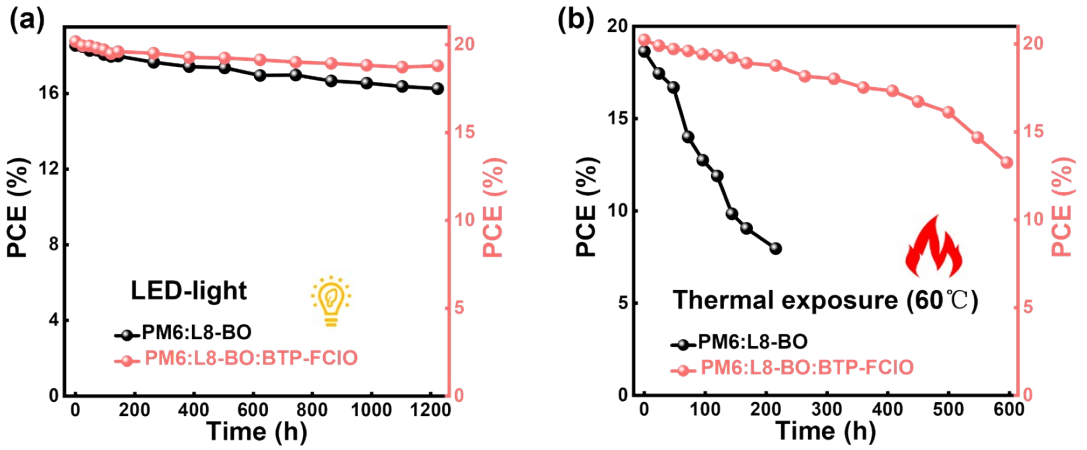

Fig. S28. (a) Operational stability of binary and ternary devices under continuous LED illumination. (b) Thermal stability of binary and ternary devices under 60°C annealing in N_2 atmosphere.

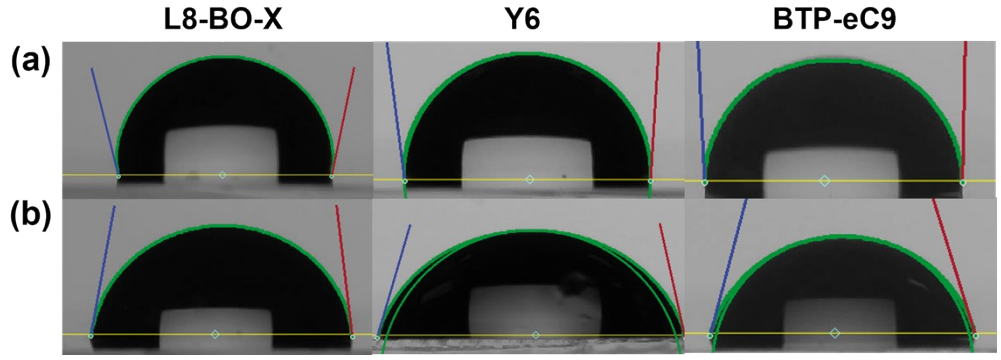

Fig. S29. Contact angle measurements for the neat films: (a) Water, (b) FA.

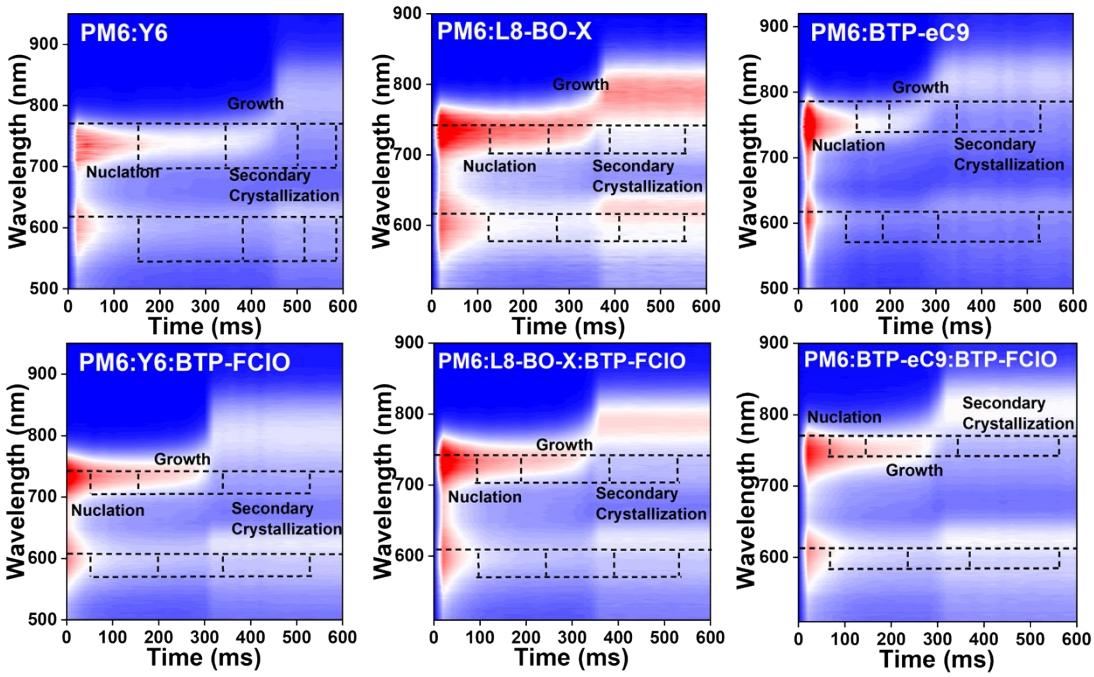

Fig. S30. 2D time-resolved in situ absorption spectra of different active layer during the solution-to-film transformation process.

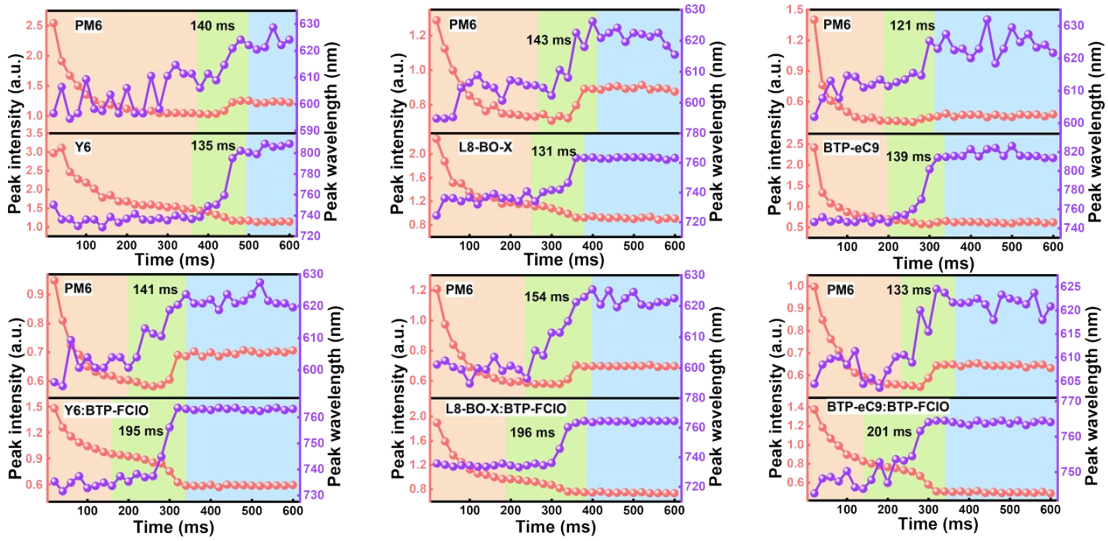

Fig. S31. Temporal evolution of peak positions for different active layer during the spin-coating process.

华南国家计量测试中心
广东省计量科学研究院
SOUTH CHINA NATIONAL CENTER OF METROLOGY
GUANGDONG INSTITUTE OF METROLOGY

校 准 证 书

CALIBRATION CERTIFICATE

证书编号 NYX202600332 第 1 页，共 4 页
Certificate No. Page of

客户名称 广西大学
Name of the Customer Guangxi University

联络信息 广西壮族自治区南宁西乡塘区大学东路100号
Contact Information No.100,Daxue East Road,Xixiangtang District,Nanning City,Guangxi,China

计量器具名称 有机太阳能电池
Description Organic Solar Cell

型号/规格 1.5 cm×1.5 cm
Model/Type

制造厂 广西大学
Manufacturer Guangxi University

出厂编号 Gui NL7077 设备管理编号 ----
Serial No. Equipment No.

接收日期 2026 年 03 月 31 日
The date of receipt Y M D

校准日期 2026 年 03 月 31 日
The date of calibration Y M D

发布日期 2026 年 04 月 08 日
The date of issue Y M D

批 准 周军红
Authorized by

核 验 林鼎添
Reviewed by

校 准 梅书刚
Calibrated by

证书专用章
Stamp

扫一扫查真伪

实验室地址：中国广东省东莞市石排镇东园大道石排段152号 邮政编码：523343
电话：+8620 86594172 投诉电话：+8620 36611242 E-mail：scm@scm.com.cn
Add: No.152, Shipai Section, Dongyuan Avenue, Shipai Town, Dongguan, Guangdong, China
Post Code:523343 Tel: +8620 86594172 Complaint Tel: +8620 36611242
证书真伪查询：www.scm.com.cn；cert.scm.com.cn Certificate AuthenticityIdentify: www.scm.com.cn；cert.scm.com.cn

说　　明

证书编号 NYX202600332
Certificate No.

DIRECTIONS

1. 本中心是国家市场监督管理总局在华南地区设立的国家法定计量检定机构，本中心的质量管理体系符合ISO/IEC 17025:2017标准的要求。

This laboratory is the National Legal Metrological Verification Institution in southern China set up by the State Administration for Market Regulation. The quality system is in accordance with ISO/IEC 17025:2017.

2. 校准地点：

The location of calibration:

东莞第二检测基地A1-403

Room A1-403, Dongguan Second Base

3. 本次校准使用的方法：

The method used:

JJF1622-2017 太阳电池校准规范：光电性能　C.S.for Solar Cells: Photoelectric Properties

4. 本证书中的校准结果可溯源至国际单位制（SI）单位和/或社会公用计量标准，本次校准使用以下计量标准器具：

The calibration results are traceable to International System of Units(SI) units and/or measurement standard for public service. The measurement standards used:

名称 Name	型号规格 Model/Type	编号 Serial No.	证书号/溯源机构 Certificate No./ Traceability to	计量特性 Metrological Characteristic
稳态太阳模拟器	SUN3000 /(300～1300)W/m²	374	NYX202500717 /本中心	光谱匹配度：A级 辐照度不均匀性：A级 辐照度不稳性：A级
标准源表	2420 /(0～60)V,(0～3)A	4051271	DBB202603297 /本中心	直流电压:U_{rel}=0.015%,(k =2) 直流电流:U_{rel}=0.015%(k =2) DCV:U_{rel}=0.1%,(k =2) DCA:U_{rel}=0.1%(k =2)
测量显微镜	15JE /(0~13)mm	023293	CYY202510474 /本中心	U=0.9μm （ k =2)
标准太阳能电池	RR_257_0 / Isc：(1～200)m A	13/01/2014	GXgf2025-03856 /国家计量院	U_{rel}=1.8%， k =2

注：1. 本证书校准结果只与受校准仪器有关。 The results relate only to the items calibrated.

Note: 2. 未经本机构书面批准，不得部分复制此证书。 This certificate shall not be reproduced except in full, without the written approval of our laboratory.

3. “客户名称”、“联络信息”由客户提供，“制造厂”、“型号规格”、“出厂编号”以及“设备编号”为仪器上标注，客户对上面内容如有异议，须在收到证书后二十个工作日内提出。

The information **Name of the Customer** and **Contact Information** are provided by customer, and the **Manufacturer**, **Model/Type**, **Serial No.** and **Equipment No.** are marked on the items.Customer shall submit any objection within 20 working days after receiving the certificate for the information above.

校 准 结 果
RESULTS OF CALIBRATION

证书编号 NYX202600332　　原始记录号 NYX202600332　　第 3 页,共 4 页
Certificate No.　　Record No.　　Page　of

1、外观检查：　符合要求
Apparent Inspection: Pass.

2、测试条件：　温度(25±2)℃；辐照度1000W/m^2。
Test conditions: Temperature: (25±2)℃；Irradiance：1000W/m^2.

3、电流-电压特性曲线和功率-电压特性曲线：
I-V and P-V curves:

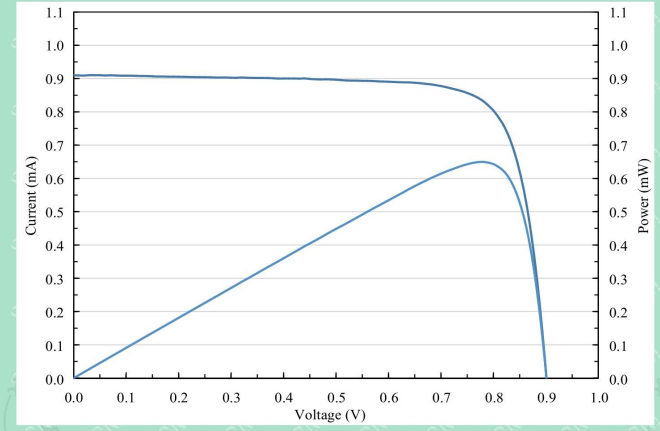

图1 电流-电压特性曲线和功率-电压特性曲线
Figure1 I-V and P-V characteristic curves

4、光电性能参数：
Results of photoelectric properties:

表1(Table 1)

面积	短路电流密度J_{sc}	短路电流I_{sc}	开路电压V_{oc}	填充因子FF	最大功率P_m	最佳工作电流I_m	最佳工作电压V_m	转换效率η
Area	Short ciruit current density	Short ciruit current	Open circuit voltage	Fill factor	Maximum power	Optimum working current	Optimum working voltage	Efficiency
cm^2	mA/cm^2	mA	V	%	mW	mA	V	%
0.0323	28.16	0.910	0.901	79.27	0.650	0.833	0.780	20.12

华南国家计量测试中心
广东省计量科学研究院
SOUTH CHINA NATIONAL CENTER OF METROLOGY
GUANGDONG INSTITUTE OF METROLOGY

校 准 结 果
RESULTS OF CALIBRATION

证书编号 NYX202600332 原始记录号 NYX202600332 第 4 页,共 4 页
Certificate No. Record No. Page of

5、被测样品信息：
Sample information:

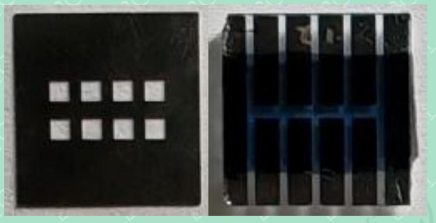

图 2 测试中使用的掩膜板及被测样品正面照片
Figure 2 Mask used during measurement and obverse side of the sample

图3 被测样品反面照片
Figure 3 Reverse side of the sample

金属掩膜板光阑平均尺寸： 1.797 mm × 1.797 mm
The average size of metal aperture mask:

说明(Note)：
1、被测样品的有效辐照面积基于对金属掩模板光阑的测量。
The effective illuminated area of the measured sample based on the measurement of metal aperture mask.
2、本次测量结果的扩展不确定度为：开路电压V_{oc}：U_{rel}=1.2%，短路电流I_{sc}：U_{rel}=2.7%，最大功率P_{max}：U_{rel}=3.0%，转换效率η：U_{rel}=3.4%，(k=2)。
The expanded uncertainty of measuring results: V_{oc}: U_{rel}=1.2%, I_{sc}: U_{rel}=2.7%, P_{max}: U_{rel}=3.0%, η:U_{rel}=3.4%, （k=2）.
3、校准活动中对测量结果有影响的条件：温度:(25±2)℃，湿度:(50±5)%RH。
Conditions under which the calibrations were made that have an influence on the measurement results: Temperature:(25±2)℃, Humidity:(50±5)%RH.
4、本证书中给出的扩展不确定度依据JJF1059.1-2012《测量不确定度评定与表示》评定，由合成标准不确定度乘以包含概率约为95%时对应的包含因子k得到。
The expanded uncertainty given in this certificate is evaluated according to JJF 1059.1-2012"*Evaluation and Expression of Uncertainty in Measurement*",which is obtained by multiplying the combined standard uncertainty by the coverage factor k corresponding to the coverage probability of about 95%.
5、该仪器的溯源日期为本证书的“校准日期”，由于复校时间间隔的长短是由仪器的使用情况、使用者、仪器本身质量等诸因素所决定的，因此，送校单位可根据实际使用情况自主决定复校时间间隔。更换重要部件、维修或对仪器性能有怀疑时，应及时校准。
The traceability date of this instrument is the "Calibration Date"on this certificate, Since the calibration interval is determined by the use of the instrument,operation of the user, the quality of the instrument itself and other factors，the re-calibration date can decided by the user according to the actual situation.In case of replacement of important parts,maintenance or doubt on the performance of the instrument,it shall be calibrated in time.

Fig. S32. Certified Efficiency of PM6:L8-BO:BTP-FClO ternary device.

Table S1. The energy levels of materials were investigated using ultraviolet photoelectron spectroscopy.

Material	Lowest unoccupied molecular orbitals (LUMO)	Highest occupied molecular orbitals (HOMO)	Optical band gaps energy (E_g)
PM6	-3.54	-5.43	1.89
L8-BO	-4.33	-5.79	1.46
BTP-FClO	-4.22	-5.73	1.51

Table S2. The peak position and crystal coherence length of three neat films.

Material	$q_{\pi\text{-}\pi}$	d-spacing (Å)	FWHM ($Å^{-1}$)	Crystalline Coherence Length (CCL)
PM6	0.32	19.82	0.094	60.16
	1.82	3.46	0.305	18.54
L8-BO	0.46	13.57	0.086	65.75
	1.87	3.36	0.222	25.47
BTP-FClO	0.49	12.72	0.070	80.78
	1.87	3.36	0.246	22.99

Table S3. Summarized Contact Angles and Surface Free Energy Parameters of the materials.

Films	Contact angle (dge)		Surface free energy, γ (mJ m^{-2})	$\chi_{D:A}$[b] ($\times10^{-2}$k)	$\chi_{A1:A2}$[b] ($\times10^{-2}$k)
	H_2O[a]	FA			
PM6	102.24	83.93	19.81	--	--
L8-BO	101.15	79.38	24.20	33.32	--
BTP-FClO	96.90	75.91	25.29	21.93	1.19
L8-BO:BTP-FClO (1:0.2)	89.64	77.92	21.24	2.45	--
L8-BO:BTP-FClO (0.8:0.4)	92.39	69.90	29.23	91.09	--
L8-BO:BTP-FClO (0.4:0.8)	93.05	73.86	25.29	33.34	--

[a]Deionized water; [b]Estimates for Flory–Huggins interaction parameter ($\chi_{donor-acceptor}$).

Table S4. Peaks and CCL of PM6:BTP-FClO, PM6:L8-BO and PM6:L8-BO:BTP-FClO in the IP directions.

Component	Peak	Peak position ($Å^{-1}$)	d-spacing (Å)	FWHM ($Å^{-1}$)	Crystalline Coherence Length (Å)
PM6:BTP-FClO	IP(010)	0.33	19.27	0.064	88.36
	IP(100)	0.37	17.17	0.110	51.41
PM6:L8-BO	IP(010)	0.32	19.88	0.038	148.81
	IP(100)	0.35	17.75	0.036	157.08
PM6:L8-BO:BTP-FClO	IP(010)	0.33	19.10	0.060	94.25
	IP(100)	0.38	16.36	0.053	106.70

Table S5. Peaks and CCL of PM6:BTP-FClO, PM6:L8-BO and PM6:L8-BO:BTP-FClO in the OOP directions.

Component	Peak	Peak position ($Å^{-1}$)	d-spacing (Å)	FWHM ($Å^{-1}$)	Crystalline Coherence Length (Å)
PM6:BTP-FClO	PM6	1.82	3.45	0.558	10.13
	BTP-FClO	1.86	3.38	0.255	22.18
PM6:L8-BO	PM6	1.76	3.57	0.260	21.75
	L8-BO	1.89	3.33	0.214	26.43
PM6:L8-BO:BTP-FClO	PM6	1.82	3.46	0.302	18.73
	L8-BO:BTP-FClO	1.92	3.27	0.223	25.36

Table S6. The statistics of hole and electron mobility in binary and ternary devices.

Photoactive layer	μ_e ($cm^2\ V^{-1}\ S^{-1}$)	μ_h ($cm^2\ V^{-1}\ S^{-1}$)	μ_e/μ_h
PM6:BTP-FClO	5.87×10^{-4}	4.74×10^{-4}	1.24
PM6:L8-BO	8.26×10^{-4}	7.51×10^{-4}	1.10
PM6:L8-BO:BTP-FClO	1.20×10^{-3}	1.13×10^{-3}	1.06

Table S7. Photovoltaic parameters of the ternary OSCs with varied L8-BO:BTP-FClO ratios under the illumination of AM 1.5G, 100 mW cm^{-2}.

PM6:L8-BO:BTP-FClO	V_{OC} [V]	$J_{SC}/J_{cal.EQE}$ [mA cm^{-2}]	FF [%]	PCE [%]
1:1.1:0.1	0.910	27.97/26.68	77.97	19.64
1:1:0.2	0.916	28.02/27.08	79.72	20.46
1:0.9:0.3	0.920	27.16/26.12	77.69	19.45
1:0.8:0.4	0.930	26.45/25.31	74.59	18.35
1:0.6:0.6	0.942	25.55/24.55	72.78	17.51
1:0.4:0.8	0.948	24.49/23.79	71.50	16.61

Table S8. Detailed device parameters of reported representative asymmetric acceptors binary OSCs.

Photoactive layer	V_{OC} (V)	J_{SC} (mA cm^{-2})	FF (%)	PCE (%)	Ref
PM6:BTP-C11-TBO	0.856	27.35	79.06	18.51	[2]
PM6:BOCl-I	0.872	28.70	78.30	19.60	[3]
PM6:BTQT-4F	0.890	26.06	78.66	18.22	[4]
PM6:2BTP2F2Cl	0.895	25.94	78.40	18.22	[5]
PM6:Qx-PhBr	0.902	26.79	81.34	19.65	[6]
PM6:BTP-g-Ar3F	0.904	25.72	74.92	17.42	[7]
PM6:Ph-2F	0.906	27.58	81.26	20.33	[8]
PM6:Ph-2Cl	0.908	26.12	80.65	19.13	[8]
PM6:LC301	0.911	24.21	78.10	17.21	[9]
PM6:X-TO1	0.913	22.39	76.50	15.63	[10]
PM6:BTP-BO-TBO	0.913	26.67	81.17	19.76	[2]
D18:H-2F	0.917	26.16	78.63	18.85	[11]
PM6:NQF	0.921	25.79	73.96	17.57	[12]
D18:H-1	0.927	25.76	77.79	18.56	[11]
PM6:PY-BO	0.929	23.33	72.26	15.66	[13]
PM6:BTP-S1	0.934	22.39	72.69	15.21	[14]

PM6:BTP-S2	0.945	24.07	72.02	16.37	[14]
PM6:TB-S	0.949	20.67	72.40	14.20	[15]
PM6:ZH2	0.956	19.94	68.29	13.03	[16]
PM6:BTP-J17	0.965	24.20	73.67	17.12	[17]
PM6:LC303	0.966	21.03	70.30	14.28	[9]
PM6:TB-S1	1.030	13.82	44.90	6.41	[15]
PM6:TB-S-O	1.120	13.62	60.00	9.09	[15]
PM6:BTP-FClO	0.990	21.54	70.93	15.13	This work

Table S9. Detailed device parameters of reported representative ternary OSCs.

Photoactive layer	V_{OC} (V)	J_{SC} (mA cm^{-2})	FF (%)	PCE (%)	Ref
PM6:L8-BO:Tri-V	0.892	27.45	81.10	19.86	[18]
PM6:L8-BO:BTP-OS	0.898	27.01	79.72	19.34	[19]
PM6:Y18:PC71BM	0.840	26.31	77.40	17.11	[20]
PM6:Y7:BTA-UD-4F	0.850	27.40	75.18	17.55	[21]
PM6:L8-BO:Y-C10ch	0.886	27.20	79.20	19.10	[22]
PTQ10:BTP-FTh:IDIC	0.870	27.17	80.60	19.05	[23]
D18:BTP-TTS:IDIC	0.879	27.55	79.30	19.22	[24]
PM6:L8-BO:BTP-EDOT-4F	0.888	26.55	78.72	18.56	[25]
PM6:N3:PC71BM	0.850	25.71	76.60	16.74	[26]
PM6:PM7:BTO	0.860	27.19	76.05	17.78	[27]
PM6:Y6:Y-4C-4O	0.870	25.42	77.00	17.03	[28]
PM6:D18:CH-FC	0.885	26.51	78.46	18.41	[29]
PM6:D18:CH-FB	0.888	26.69	80.03	18.97	[29]
PM6:D18:CH-CB	0.901	26.22	77.07	18.21	[29]
PM6:BTP-eC9:BTP-BO-3FO	0.857	28.13	79.80	19.24	[30]
PM6:Y6:BTP-M	0.875	26.56	73.46	17.03	[31]

PM6:CH-BBQ:BO-4Cl	0.882	27.05	79.40	18.94	[32]
PM6:CH-ThCl:CH-6F	0.931	26.20	77.09	18.80	[33]
PM6:BTP-eC9:BTP-2FClO	0.863	27.96	80.15	19.34	[1]
PM6:L8-BO:BTP-FClO	0.916	28.02	79.72	20.46	This work

Table S10. The fitting parameters from Nyquist and Mott-Schottky plots.

Active layer	R_S (Ω)	R_{CT} (Ω)	CPE-T (nF)	CPE-P	V_{bi} (V)
PM6:BTP-FClO	149	1881	4.425	0.776	0.83
PM6:L8-BO	86	1064	5.027	0.967	0.87
PM6:L8-BO:BTP-FClO	82	792	6.152	0.971	0.91

Table S11. Summarizes the dispersion bimolecular recombination fitting parameters.

Photoactive layer	n_0 (cm^{-3})	γ	τ_b (10^{-5} μs)	β (10^{-12} cm^3 s^{-1})
PM6:BTP-FClO	6.26×10^{16}	0.66	3.34	4.90
PM6:L8-BO	6.62×10^{16}	0.81	2.25	2.43
PM6:L8-BO:BTP-FClO	8.25×10^{16}	0.94	1.93	0.95

Table S12. Summarized Contact Angles and Surface Free Energy Parameters of the materials.

Films	Contact angle (dge)		Surface free energy, γ (mJ m^{-2})	$\chi_{D:A}$[b] ($\times10^{-2}$k)	$\chi_{A1:A2}$[b] ($\times10^{-2}$k)
	H_2O[a]	FA			
PM6	102.24	83.93	19.81	--	--
BTP-FClO	96.90	75.91	25.29	21.93	1.19
Y6	95.42	75.57	24.67	27.49	0.28
L8-BO-X	102.92	81.41	23.07	12.37	5.08
BTP-eC9	91.91	73.98	24.66	26.48	0.39

[a]Deionized water; [b]Estimates for Flory–Huggins interaction parameter ($\chi_{donor-acceptor}$).

References

1 B. Zou, A. Liang, P. Ding, J. Yao, X. Zeng, H. Li, R. Ma, C. Li, W. Wu, D. Chen, M. Qammar, H. Yu, J. Yi, L. Guo, S. H. Pun, J. E. Halpert, G. Li, Z. Kan, H. Yan, *Angewandte Chemie,* 2025, **137**, e202415332.

2 J. Guo, S. Qin, J. Zhang, C. Zhu, X. Xia, Y. Gong, T. Liang, Y. Zeng, G. Han, H. Zhuo, Y. Li, L. Meng, Y. Yi, J. Chen, X. Li, B. Qiu, Y. Li, *Nat. Commun.,* 2025, **16**, 1503.

3 H. Rong, P. Ding, S. Qin, Z. Chen, D. Liu, F. Wang, K. Ma, Y. Hu, D. Qian, Z. Ge, *ACS Energy Lett.,* 2025, **10**, 393.

4 H. Zhang, Y. Chai, J. Zhao, E. Zhu, Y. Chen, L. Liu, D. M. Guldi, *Adv. Energy Mater.* **2025**, 2500332.

5 W. Zhou, J. Liu, J. Deng, F. Wu, F. Yu, Y. Zhang, Y. Zhang, S. Y. Jeong, H. Y. Woo, L. Chen, *ACS Energy Lett.,* 2025, **10**, 3993.

6 D. Qiu, L. Zhang, H. Zhang, A. Tang, J. Zhang, Z. Wei, K. Lu, *J. Mater. Chem. A,* 2025, **13**, 4237.

7 Z. Li, Z. Xu, S. Chen, J. Yao, H. Fu, M. Zhang, Y. Bai, H. Wang, Z. Liu, Z.-G. Zhang, *J. Mater. Chem., A* 2023, **11**, 4539.

8 J. Liu, Z. Suo, L. Li, W. Zhao, J. Huo, J. Chen, G. Long, Z. Yao, C. Li, X. Wan, Y. Chen, *Energy Environ. Sci.,* 2025, **18**, 8658-8666.

9 C. Li, G. Lu, H. S. Ryu, X. Sun, H. Y. Woo, Y. Sun, *ACS Appl. Mater. Interfaces,* 2022, **14**, 43207.

10 W. Xiang, X. Xu, Y. Huang, L. Yu, R. Li, Y. Jiang, Q. Peng, *Chem. Eng. J.,* 2022, **441**, 136058.

11 Q. Han, W. Shi, W. Zhao, T. He, R. Wang, G. Long, Z. Yao, B. Kan, Y. Lu, X. Wan, C. Li, Y. Chen, *Adv. Optical Mater.,* 2025, **13**, 2500450.

12 J. Wang, H. Chen, X. Xu, Z. Ma, Z. Zhang, C. Li, Y. Yang, J. Wang, Y. Zhao, M. Zhang, X. Wan, Y. Lu, Y. Chen, *J. Mater. Chem. A,* 2022, **10**, 16714.

13 J. Wang, C. Sun, Y. Li, F. Bi, H. Jiang, C. Yang, X. Bao, J. Chu, *Nat. Commun.* 2025, **16**, 1784.

14 S. Li, L. Zhan, Y. Jin, G. Zhou, T. Lau, R. Qin, M. Shi, C. Li, H. Zhu, X. Lu, F. Zhang, H. Chen, *Adv. Mater.* 2020, **32**, 2001160.

15 L. Xie, A. Lan, Q. Gu, S. Yang, W. Song, J. Ge, R. Zhou, Z. Chen, J. Zhang, X. Zhang, D. Yang, B. Tang, T. Wu, Z. Ge, *ACS Energy Lett.,* 2023, **8**, 361.

16 Y. Zhang, J. Deng, S. You, X. Huang, J. Liu, Y. Cheng, B. Huang, X. Chen, Z. Sun, C. Yang, Q. Cao, F. Wu, L. Chen, *Adv. Funct. Mater.,* 2024, **34**, 2308151.

17 Z. Ling, J. Wu, J. P. Jurado, C. E. Petoukhoff, S. Y. Jeong, D. Naphade, M. Babics, X. Chang, H. Faber, S. Doukas, E. Lidorikis, M. I. Nugraha, M. He, M. Alqurashi, Y. Lin, X. Sun, H. Hu, H. Y. Woo, S. De Wolf, L. Tsetseris, F. Laquai, D. Yu, E. Wang, T. D. Anthopoulos, *Materials Science and Engineering: R: Reports,* 2025, **163**, 100922.

18 J. Song, C. Zhang, C. Li, J. Qiao, J. Yu, J. Gao, X. Wang, X. Hao, Z. Tang, G. Lu, R. Yang, H. Yan, Y. Sun, *Angewandte Chemie,* 2024, **63**, e202404297.

19 W. Liang, S. Zhu, K. Sun, J. Hai, Y. Cui, C. Gao, W. Li, Z. Wu, G. Zhang, H. Hu, *Adv. Funct. Mater.* 2025, **35**, 2415499.

20 J. Mao, J. Iocozzia, J. Huang, K. Meng, Y. Lai, Z. Lin, *Energy Environ. Sci.,* 2018, **11**, 772.

21 T. Gokulnath, R. Durga Gayathri, H.-Y. Park, J. Kim, H. Kim, J. Kim, S. Sudhaker Reddy, J. Yoon, S.-H. Jin, *Chem. Eng. J.,* 2022, **448**, 137621.

22 C. Xiao, X. Wang, T. Zhong, R. Zhou, X. Zheng, Y. Liu, T. Hu, Y. Luo, F. Sun, B. Xiao, Z. Liu, C. Yang, R. Yang, *Adv. Sci.,* 2023, **10**, 2206580.

23 K. Chong, X. Xu, H. Meng, J. Xue, L. Yu, W. Ma, Q. Peng, *Adv. Mater.,* 2022, **34**, 2109516.

24 G. Wu, X. Xu, C. Liao, L. Yu, R. Li, Q. Peng, *Small,* 2023, **19**, 2302127.

25 M. Deng, X. Xu, Y. Duan, L. Yu, R. Li, Q. Peng, *Adv. Funct. Mater.,* 2023, **33**, 2212290.

26 K. Jiang, Q. Wei, J. Y. L. Lai, Z. Peng, H. K. Kim, J. Yuan, L. Ye, H. Ade, Y. Zou, H. Yan, *Joule,* 2019, **3**, 3020.

27 W. Sun, H. Chen, B. Zhang, Q. Cheng, H. Yang, Z. Chen, G. Zeng, J. Ding, W. Chen, Y. Li, *Chin. J. Chem.,* 2022, **40**, 2963.

28 X. Yang, G. Ye, K. Tran, Y. Liu, J. Cao, J. Dong, G. Portale, J. Liu, P. Zhang, M. A. Loi, R. C. Chiechi, L. J. A. Koster, *ACS Materials Lett.,* 2024, **6**, 1207.

29 H. Liang, H. Chen, Y. Zou, Y. Zhang, Y. Guo, X. Cao, X. Bi, Z. Yao, X. Wan, Y. Chen, *Chem. Commun.,* 2023, **59**, 13367.

30 B. Zou, W. Wu, T. A. Dela Peña, R. Ma, Y. Luo, Y. Hai, X. Xie, M. Li, Z. Luo, J. Wu, C. Yang, G. Li, H. Yan, *Nano-Micro Lett.,* 2023, **16**, 30.

31 L. Zhan, S. Li, T.-K. Lau, Y. Cui, X. Lu, M. Shi, C.-Z. Li, H. Li, J. Hou, H. Chen, *Energy Environ. Sci.,* 2020, **13**, 635.

32 T. Duan, W. Feng, Y. Li, Z. Li, Z. Zhang, H. Liang, H. Chen, C. Zhong, S. Jeong, C. Yang, S. Chen, S. Lu, O. A. Rakitin, C. Li, X. Wan, B. Kan, Y. Chen, *Angewandte Chemie,* 2023, **135**, e202308832.

33 X. Si, Y. Huang, W. Shi, R. Wang, K. Ma, Y. Zhang, S. Wu, Z. Yao, C. Li, X. Wan, Y. Chen, *Adv. Funct. Mater.,* 2023, **33**, 2306471.

34 C. Xu, J. Yang, S. Gámez-Valenzuela, J.-W. Lee, J. Che, P. Chen, G. Zhang, D. Hu, Y. Wang, J. Lv, Z. Zhong, X. Chen, G. Zhang, F. Zhao, B. J. Kim, X. Guo, B. Liu, *Energy Environ. Sci.* 2025, **18**, 5913.

35 K. Xing, D. Cai, D. Wang, J.-Y. Wang, C. Tang, Y. Ma, Q. Zheng, *National Science Review,* 2025, **12**, nwaf089.

36 B. Zhao, L. Zhu, S. Xiong, J. Yu, X. Wang, J. Zhao, L. Tan, J. Zhang, J. Zhong, L. Kan, X. Wan, K. Jiang, H. Li, Z. Ma, Y. Liu, H. Zhu, Z. Kan, F. Liu, Z. Sun, J. Chu, Q. Bao, *Adv. Energy Mater.,* 2025, **15**, e04947.